Desalination and Water Treatment
www.deswater.com
doi: 10.1080/19443994.2015.1089419

57 (2016) 18248–18259
August

Taylor & Francis
Taylor & Francis Group

Thermodynamic study of magnesium sulfate crystallization: application of Pitzer model and quinary diagrams

Ferid Hajbi[a,*], Halim Hammi[a], Roland Solimando[b], Adel M'nif[a]

[a]*National Centre of Research in Materials Science, Technologic Park of Borj Cedria, Soliman B.P. 73–8027, Tunisie, Tel. +216 79 32 54 70; Fax: +216 79 32 53 14; emails: feridhajbi@gmail.com (F. Hajbi), halim_hammi@yahoo.com (H. Hammi), mnif.adel@inrst.rnrt.tn (A. M'nif)*
[b]*Reactions and Process Engineering Laboratory, ENSIC, 1,Rue Grandville, Nancy BP 20451, France, email: roland.solimando@ensic.inpl-nancy.fr*

Received 10 February 2015; Accepted 24 August 2015

ABSTRACT

Extracting valuable salts from reverse osmosis reject brine may be a solution to reduce environmental risk of this effluent if discarded. Isothermal evaporation (25°C) allows recovering many salts like gypsum, halite, and magnesium salts (epsomite, hexahydrite). In this paper, magnesium sulfate crystallization was studied, for this purpose two different quinary diagrams were used to draw the crystallization path. Furthermore, the application of Pitzer model and the use of Phreeqc program were required, respectively, to calculate electrolytes solubility product and to simulate the evaporation steps. Experimentally, X-ray diffraction was adopted to identify the nature of recovered solid phases. The different results of this study are almost similar and confirm the crystallization of epsomite and hexahydrite at the end of evaporation process.

Keywords: Reverse osmosis; Evaporation; Quinary diagrams; Pitzer model; Phreeqc

1. Introduction

Concentrate rejected from the reverse osmosis desalination plant may present many environmental hazards, as mentioned by Khordagui [1], Dweiri and Badran [2]. In order to valorize this effluent, the extraction of dissolved salts is required; M. Ahmed et al. [3], J.M. Arnal and colleagues [4] studied the feasibility of salt production from RO desalination plant.

In this paper, we are interested in recovering magnesium salts from RO desalination pilot plant located in Sousse (northeast of Tunisia) which produces wastewater with TDS level exceeding 60 g L^{-1}. In fact, epsomite (Mg $SO_4 \cdot 7H_2O$) and hexahydrite (Mg $SO_4 \cdot 6H_2O$) are among the most valuable chemical resources extracted from brines, they can lead to magnesium oxide which is very useful in industry [5]. For this purpose, isothermal evaporation (25°C) was performed at laboratory scale in order to obtain a fairly complete progression of evaporation brines [6].

During evaporation, a set of brine samples of various densities was collected and analyzed to determine the crystallization's sequences of solid phases. Given the main composition of the brine is relatively complex (Na–K–Mg–Ca–Cl–SO_4), Pitzer model and quinary diagrams are the different adopted methods in order to predict the crystallization of epsomite and

*Corresponding author.

hexahydrite [7]. Also the use of Phreeqc program was also helpful to simulate evaporation steps. The recovered salts were analyzed by X-ray diffraction technique to confirm theoretical studies results.

2. Materials and methods

The process used in this work is the evaporation of the studied brine in a pilot of 6 L at isothermal condition (25°C) (Fig. 1). Each time when there was a density variation (10^{-2} g/cm^3), a levy of 5 ml of solution was made to use for chemical analysis. The initial volume decreases gradually, different salts precipitate sequentially and settle at the bottom of the crystallizer, samples of these solids are taken for physical and chemical analysis (Fig. 2).

Equipment used for this work is listed below:

(1) Thermostatic bath fixed at 25°C.
(2) Crystallizer for brine evaporation.
(3) Filtration equipment (vacuum pump, Buchner, and vacuum flask).

Liquid density was determined by the measurement of buoyancy (Archimedes force) using a precision balance (accuracy at 0.1 mg). K^+ and Na^+ ions concentrations were analyzed by a spectrophotometer using a Jenway PFP7 instrument. Mg^{2+} and Ca^{2+} ions concentrations were determined by EDTA complexometric titration. Chloride concentration was measured by potentiometric analysis device Titrino DMS 716 consisting of a potentiometer and a silver electrode and using silver nitrate solution. The SO_4^{2-} ion concentration was determined gravimetrically. Solid phases were removed daily by filtration and characterized by chemical analysis and XRD using a Philips PW 3040 generator, PW 3050/60 h/2 h goniometer, and PW 3373/00 copper cathode.

3. Thermodynamic modeling

The thermodynamics of multicomponent solutions has been successfully treated using a semi empirical model based upon a virial series (in molality) and an extended Debye–Hückel term [8,9]. For systems at higher aqueous concentration, and for miscible fused salts, an alternative mole fraction-based model was developed by Pitzer [10] and Pitzer and Simonson [11] for mixtures containing ions of symmetrical charge type. The excess Gibbs energy of the mixed solution is assumed to consist of two components: short-range force terms accounted for by a Margules expansion in concentration and a long-range force (Debye–Hückel term) that is a function only of the ionic strength of the solution (at constant temperature and pressure). In this paper, Pitzer model of activity coefficient γ in multicomponent electrolyte solutions is used to compute the ion activity products (IAPs) of potentially important solid phases recovered from brine evaporation specially epsomite and hexahydrite [12].

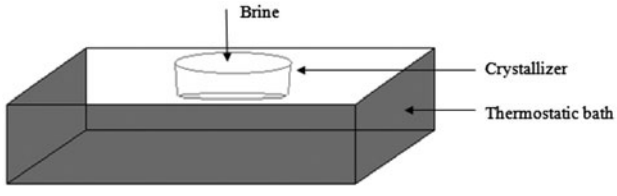

Fig. 1. Experimental set of isothermal evaporation.

The Pitzer equation has been given in many papers as well as recent reviews [13,14], in our case, we have used the formulation (Eqs. (1) and (2)) given by Harvie and Weare [15].

For the cation M:

$$\ln \gamma_M = z_M^2 F + \sum_a m_a(2B_{M_a} + ZC_{M_a}) + \sum_c m_c(2\phi_{Mc} + \sum_a m_a\psi_{Mca}) + \sum_{a<a'}\sum m_a m_{a'}\psi_{aa'M} + z_M \sum_c \sum_a m_c m_a C_{ca} \quad (1)$$

For the anion X:

$$\ln \gamma_X = z_X^2 F + \sum_a m_c(2B_{cX} + ZC_{cX}) + \sum_a m_a(2\phi_{Xa} + \sum_c m_c\psi_{Xac}) + \sum_{c<c'}\sum m_c m_{c'}\psi_{cc'X} + z_X \sum_c \sum_a m_c m_a C_{ca} \quad (2)$$

In these equations, m_i is the molality of ion I, with M, c, and c´ referring to cations and X, a, and a´ referring to anions.

Z is given by:

$$Z = \sum_i |z_i| \times m_i \quad (3)$$

F is a function summing the D–H equation and additional terms (Eq. (4)):

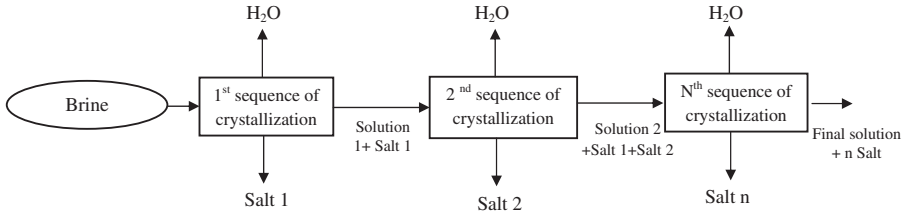

Fig. 2. Methodology of brine isothermal evaporation.

$$F = -A^{\phi}\left[\frac{\sqrt{I}}{(1+b\sqrt{I})} + \left(\frac{2}{b}\right)\ln(1+b\sqrt{I})\right] + \sum_{c}\sum_{a} m_c m_a B'_{ca} + \sum_{c<c'}\sum m_c m'_c \phi_{cc'} + \sum_{a<a'}\sum m_a m_{a'} \phi'_{aa'} \quad (4)$$

I is the molal ionic strength, defined by Eq. (5):

$$I = \frac{1}{2}\sum z_i^2 m_i \quad (5)$$

The Debye–Hückel parameter A^{ϕ} used in these equations is numerically smaller that in the usual D–H equation (Eq. (6)):

$$A^{\phi} = \frac{1}{3}(2\pi N_A \rho_0/1000)^{\frac{1}{2}}\left[\frac{e^2}{\varepsilon_0 kT}\right]^{\frac{3}{2}} \quad (6)$$

where N_A is Avogadro's constant, e is the electronic charge, k is the Boltzmann constant, and ρ_0 and ε_0 are the density and dielectric constant of pure water.

For electrolytes in which one or both ions are univalent:

$$B_{MX} = \beta^{(0)}_{MX} + \beta^{(1)}_{MX} g(\alpha\sqrt{I}) \quad (7)$$

$$B'_{MX} = \beta^{(1)}_{MX} g'(\alpha\sqrt{I})/I \quad (8)$$

α is assigned a value of 2.

For electrolytes of higher valences such as 2:2.

$$B_{MX} = \beta^{(0)}_{MX} + \beta^{(1)}_{MX} g(\alpha_1\sqrt{I}) + \beta^{(2)}_{MX} g(\alpha_2 I^{1/2}) \quad (9)$$

$$B'_{MX} = \beta^{(1)}_{MX} g'(\alpha_1\sqrt{I})/I + \beta^{(2)}_{MX} g'(\alpha_2 I^{1/2})/I \quad (10)$$

For these higher valence electrolytes $\alpha_1 = 1.4$ and $\alpha_2 = 12$.

Functions g and g´ have the following form:

$$g(x) = 2[1-(1+x)e^{-x}]/x^2 \quad (11)$$

$$g'(x) = -2\left[1-\left(1+x+(1/2)x^2\right)e^{-x}\right]/x^2 \quad (12)$$

With $x = \alpha I^{1/2}$

The parameter C_{MX} in Eq. (13) is related to tabulated parameters derived from data in aqueous single-salt systems.

$$C_{MX} = \frac{C^{\Phi}_{MX}}{2\sqrt{z_M z_X}} \quad (13)$$

The $\beta^{(0)}_{MX}$, $\beta^{(1)}_{MX}$, and $\beta^{(2)}_{MX}$ terms represent specific interaction parameters for the pure electrolytes, Φ is the second virial coefficient for the mixed solution, (Φ') corresponds to the derivative ($\partial\Phi/\partial I$), C is the third virial coefficient for the pure electrolyte, and (ψ) is its corresponding for the mixed solution, all these parameters are available in the literature (Marion[16] Pitzer [17] and Felmy [18]).

4. PHREEQC interactive program

PHREEQC is a computer program for simulating chemical reactions and transport processes in natural or polluted water, PHREEQC is based on the Fortran program PHREEQE (Parkhurst and others, 1980). The program is based on equilibrium chemistry of aqueous solutions interacting with minerals, gasses, solid solutions, exchangers, and sorption surfaces. The program's database of Pitzer interaction parameters includes a partially validated database at 25℃ for the system Na-K-Mg–Ca–H–Cl-SO_4–OH–HCO_3–CO_3–$C0_2$–H_2O (Appendix 1).

In our work, brine evaporation is accomplished by removing water from the chemical system, to attain a specified saturation index for a pure phase. This step

was repeated, water content decreases progressively which leads to an increase in the saturation of the solution and so IAP of some electrolytes can reach the value of the solubility product *K*s.

5. Quinary diagrams

5.1. Jänecke projection

An equilibrium diagram is a geometric representation (two- or three-dimension) of equilibrium states in a thermodynamic system. Such representation indicates the present phases in the system and their stability fields. In the case of quinary diagram, we used the Jänecke representation which consists in supposing that the solution is concentrated on NaCl, each surface can be labeled with a single phase (halite + solution are always present), lines formed by the intersection of two surfaces have two-phase label and invariant point has a three-phase label [19,20]. Table 1 includes all the abbreviations of solid phases present in the two studied diagrams.

5.2. Crystallization path

The crystallization path is the progress of physical transformations caused by the loss or the addition of a constituent through a given solubility phase diagram. During the system's evolution, the number, the nature, the composition, and the relative quantity of different condensed phases can be defined. In the case of isothermal evaporation of saturated solution, the constituent that disappears from water leads to crystals deposit and to constitution changes.

The representative point of the equilibrium solution moves in the diagram, it describes a certain line which is called crystallization path.

Table 1
Minerals abbreviations

Chemical formula	Abbreviation	Mineralogical name
$CaSO_4$	A	Anhydrite
$3K_2SO_4{\cdot}Na_2SO_4$	Ap	Aphthialite (Glaserite)
$CaCl_2{\cdot}6H_2O$	Ant	Antarcticite
$MgCl_2{\cdot}6H_2O$	Bi	Bishofite
$Na_2\ Mg(SO_4)_2{\cdot}4H_2O$	Bl	Bloedite
$KMgCl_3{\cdot}6H_2O$	Car	Carnallite
$MgSO_4{\cdot}7H_2O$	Ep	Epsomite
$CaSO_4{\cdot}2H_2O$	G	Gypsum
$Na_2Ca(SO_4)_2$	Gl	Glauberite
NaCl	H	Halite
$MgSO_4{\cdot}6H_2O$	Hx	Hexahydrite
$KCl.MgSO_4{\cdot}3H_2O$	Ka	Kainite
$MgSO_4{\cdot}H_2O$	Ki	Kiéserite
$K_2\ Mg(SO)_2{\cdot}4H_2O$	Le	Leonite
KCl	Syl	Sylvite
$Mg_2CaCl_6{\cdot}12H_2O$	Tc	Tachyhydrite
Na_2SO_4	Th	Thenardite

6. Results and discussion

6.1. Calculation of IAP

As mentioned above, Pitzer model was used to predict the salts which can be crystallized; by calculating the IAP for various phases in these solutions:

$$\mathrm{IAP}(c_{\upsilon c}a_{\upsilon a}\cdot\upsilon_w H_2O)=a_c^{\upsilon c}.a_a^{\upsilon a}.a_w^{\upsilon w} \quad (14)$$

where υ_c mol of cation "c", υ_a mol of anion "*a*", and υ_w mol of water "w".

Through this study, we calculated the activity coefficient of each element during evaporation referring

Table 2
Initial ionic composition of brine

Ions	Na^+	Ca^{2+}	Mg^{2+}	K^+	Cl^-	SO_4^{2-}
Molality (mol/kg)	0.651 ± 0.008	0.017 ± 0.002	0.090 ± 0.003	0.017 ± 0.002	0.816 ± 0.01	0.047 ± 0.003

Table 3
Evolution of log (IAP) of epsomite and hexahydrite during evaporation

	log IAP			
	Epsomite		Hexahydrite	
Density	Experimental	Phreeqc	Experimental	Phreeqc
1.0493	−4.23	−4.25	−4.21	−4.23
1.0518	−4.16	−4.20	−4.15	−4.19
1.0551	−4.09	−4.16	−4.07	−4.14
1.0625	−4.02	−4.09	−4.00	−4.07
1.0829	−3.98	−3.97	−3.96	−3.94
1.0960	−3.64	−3.76	−3.61	−3.73
1.1215	−3.51	−3.58	−3.46	−3.53
1.1500	−3.32	−3.43	−3.26	−3.44
1.2112	−2.85	−2.98	−2.76	−2.94
1.2369	−2.58	−2.58	−2.44	−2.44
1.2400	−2.55	−2.68	−2.41	−2.54
1.2422	−2.42	−2.46	−2.27	−2.32
1.2584	−2.34	−2.18	−2.16	−1.9
1.2720	−2.24	−2.10	−2.05	−1.82
1.2910	−1.84	−1.88	−1.64	−1.68
1.3010	−1.93	−1.88	−1.72	−1.64

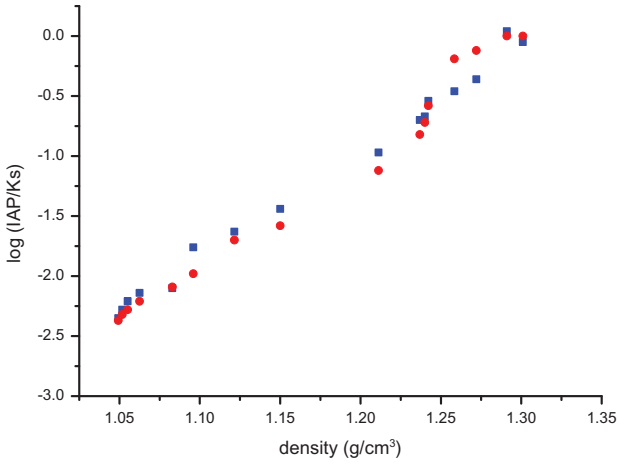

Fig. 3. Variation of log IAP/Ks (Epsomite) with density: (■) Experimental and (●) Phreeqc.

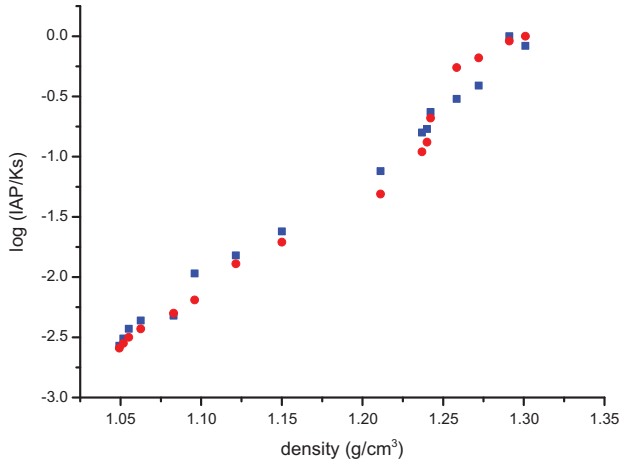

Fig. 4. Variation of log IAP/Ks (Hexahydrite) with density: (■) Experimental and (●) Phreeqc.

to an experimental analysis which allowed the ion activity calculation. At the same time, this parameter was determined by an evaporation simulation (Phreeqc Program).

To simulate all evaporation's steps, major ions concentrations of initial solution were determined (Table 2), this composition then changes according to the amount of evaporated solvent.

Comparing the IAP (experimental and simulated) to solubility products of epsomite and hexahydrite at 25°C (given in the literature), leads to estimating the possibility of their crystallization.

The evolution of (log IAP) of epsomite and hexahydrite according to density was summarized in Table 3.

Results presented in Fig. 3 show the evolution of log (IAP/*Ks*) of epsomite during evaporation, curves

Table 4
Coordinate of crystallization path in quinary systems at 25°C

System Na^+, K^+, Mg^{2+}/Cl^-, SO_4^{2-}/H_2O						Phases crystallized	System Na^+, Mg^{2+}, Ca^{2+}/Cl^-, SO_4^{2-}/H_2O						Phases crystallized
Experimental			Phreeqc				Experimental			Phreeqc			
K_2 (%)	Mg (%)	SO_4 (%)	K_2 (%)	Mg (%)	SO_4 (%)		Ca (%)	Mg (%)	SO_4 (%)	Ca (%)	Mg (%)	SO_4 (%)	
5.95	61.81	32.24	5.95	61.81	32.24	Bloedite	11.33	58.27	30.40	11.33	58.28	30.39	Anhydrite
5.89	62.66	31.45	5.94	61.82	32.24	Bloedite	11.95	58.63	29.42	11.33	58.28	30.39	Anhydrite
6.92	62.76	30.32	5.95	61.81	32.24	Bloedite	11.22	59.86	28.92	11.33	58.27	30.40	Anhydrite
6.70	63.81	29.49	5.94	61.83	32.23	Bloedite	11.57	60.48	27.95	11.33	58.29	30.38	Anhydrite
6.90	64.51	28.59	5.95	61.81	32.24	Bloedite	13.30	60.08	26.63	11.33	58.27	30.40	Anhydrite
5.86	62.92	31.21	6.03	62.69	31.28	Bloedite	9.71	60.35	29.94	10.28	59.85	29.87	Anhydrite
6.32	63.67	30.02	6.42	66.74	26.84	Bloedite	6.80	63.34	29.86	5.09	67.69	27.22	Anhydrite
5.64	69.52	24.84	6.44	66.98	26.58	Bloedite	3.78	70.89	25.33	4.75	68.19	27.06	Anhydrite
6.09	69.51	24.40	6.62	68.82	24.56	Bloedite	1.49	72.91	25.60	2.15	72.11	25.74	Anhydrite
5.19	70.62	24.19	6.70	69.68	23.62	Bloedite	0.61	74.03	25.36	0.88	74.02	25.10	Anhydrite
7.04	70.24	22.72	6.73	69.96	23.31	Bloedite	0.28	75.34	24.37	0.45	74.68	24.88	Anhydrite
6.04	70.95	23.01	6.76	70.30	22.94	Bloedite	0.18	75.37	24.44	0.20	75.24	24.56	Anhydrite
7.70	69.89	22.41	6.71	70.54	22.75	Bloedite	0.00	75.72	24.28	0.04	75.59	24.37	Anhydrite
6.72	70.09	23.19	6.71	70.56	22.73	Epsomite	0.00	75.14	24.86	0.02	75.62	24.36	Epsomite
5.78	76.46	17.76	5.63	75.29	19.08	Epsomite	0.00	81.15	18.85	0.01	79.78	20.21	Epsomite
4.89	82.02	13.09	5.11	82.27	12.61	Hexahydrite	0.00	86.24	13.76	0.00	86.70	13.29	Hexahydrite

of experimental and simulated values are almost similar, the density varies from 1.0493 to 1.3010; log *Ks* of epsomite at 25°C is equal to −1.88 (A. Droubi, B. Fritz, and Y. Tardy [21], the solution reaches saturation on epsomite when IAP and *Ks* are equalized (log IAP/*Ks* = 0) at the end of evaporation (d = 1.2910 g/cm^3).

In Fig. 4, the experimental and simulated results of hexahydrite are plotted according to solution density, IAP attains *Ks* (log *Ks* = −1.64) [21] at the same density of epsomite deposit (d = 1.2910).

The use of Phreeqc program confirms results obtained experimentally.

6.2. Crystallization path

Two types of path are studied: experimental and simulated by Phreeqc program. The coordinates of the studied solution in the different diagrams were determined referring to concentrations of elements present in brine and then summarized in Table 4.

6.2.1. Quinary diagram Na^+, K^+, Mg^{2+}/Cl^-, SO_4^{2-}/H_2O

The quinary diagram Na^+, K^+, Mg^{2+}/Cl^-, SO_4^{2-}/H_2O is free of calcium, it contains 13 invariant points, the figurative point (calculated and simulated)

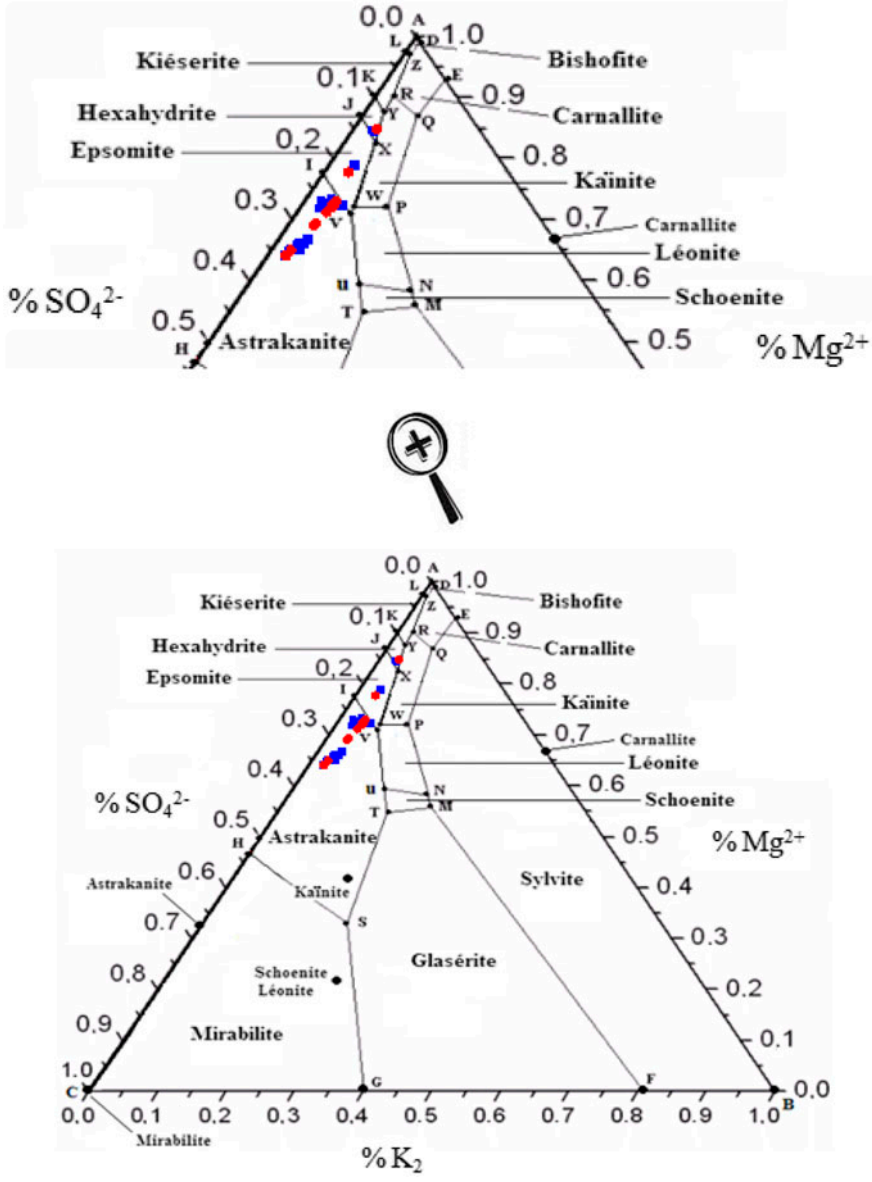

Fig. 5. Crystallization path for the system Na^+, K^+, Mg^{2+}/Cl^-, SO_4^{2-}/H_2O: (■) Experimental and (●) Phreeqc.

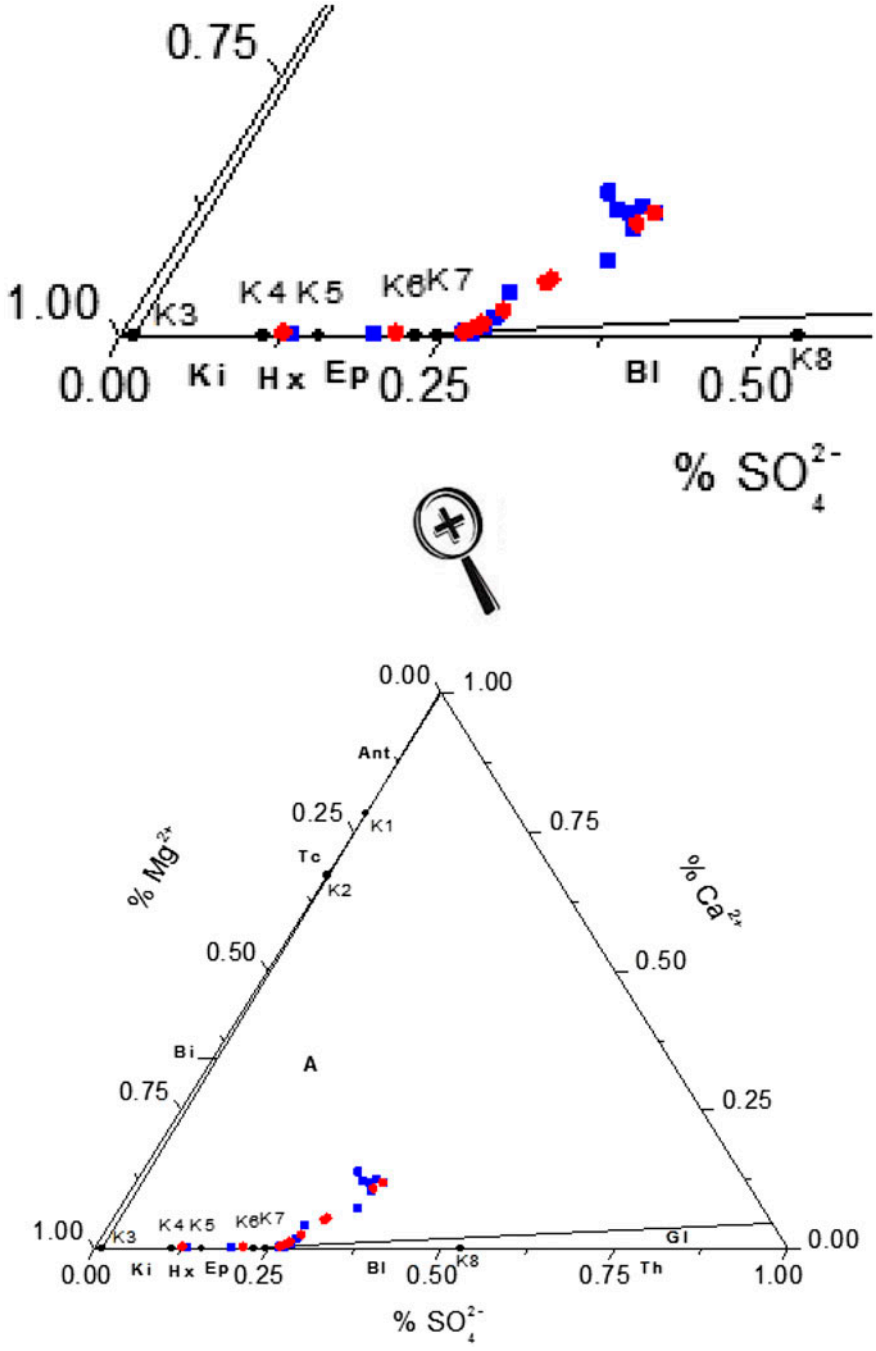

Fig. 6. Crystallization path for the system Na^+, Mg^{2+}, Ca^{2+}/Cl^-, SO_4^{2-}/H_2O: (■) Experimental and (●) Phreeqc.

of solution before evaporation is situated at the field of bloedite. The crystallization path plotted in this diagram for different steps of evaporation is calculated as follows:

$$\%\,K_2 = \frac{\frac{n_{K^+}}{2}}{\frac{n_{K^+}}{2} + n_{Mg^{2+}} + n_{SO_4^{2-}}} \times 100 \quad (15)$$

$$\%\,Mg = \frac{n_{Mg^{2+}}}{\frac{n_{K^+}}{2} + n_{Mg^{2+}} + n_{SO_4^{2-}}} \times 100 \quad (16)$$

$$\%\,SO_4 = \frac{n_{SO_4^{2-}}}{\frac{n_{K^+}}{2} + n_{Mg^{2+}} + n_{SO_4^{2-}}} \times 100 \quad (17)$$

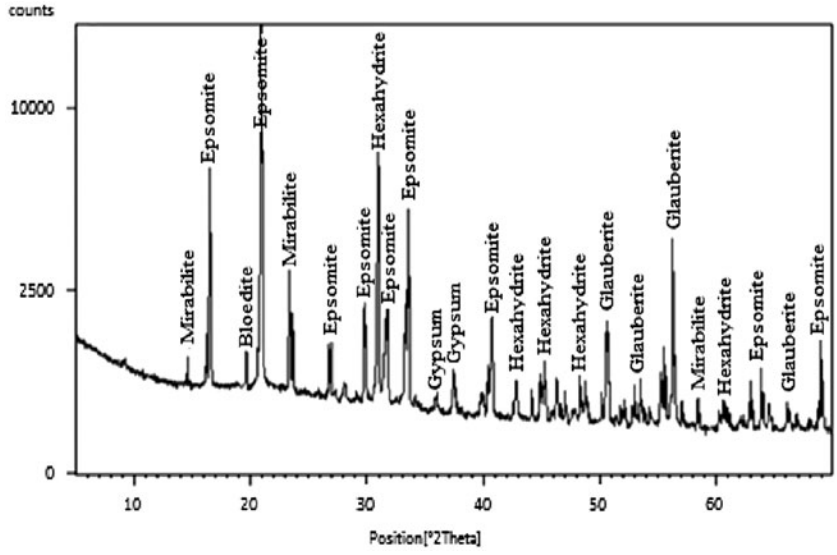

Fig. 7. Diffractogram of recovered salts.

According to Fig. 5, it can be noted that simulated and experimental pathways progress in the same direction until the invariant point *X*; the predicted mineral phases along the pathway should appear in sequences as follows: halite + bloedite, halite + epsomite, and halite + hexahydrite. The solution is entirely desolvated before reaching the phase kieserite.

6.2.2. Quinary diagram Na^+, Mg^{2+}, Ca^{2+}/Cl^-, SO_4^{2-}/H_2O

This system ignores potassium content, it contains eight invariant points and is dominated by anhydrite phase where the figurative point of initial solution is located; during evaporation, the crystallization path starts from the anhydrite field until reaching the domain of epsomite or hexahydrite with existence of halite in the majority of the process (Fig. 6). This diagram shows in a very clear way that simulated and experimental paths are similar. The percentage of each element during evaporation is calculated as follows:

$$\%\,\mathrm{Ca} = \frac{n_{Ca^{2+}}}{n_{Ca^{2+}} + n_{Mg^{2+}} + n_{SO_4^{2-}}} \times 100 \quad (18)$$

$$\%\,\mathrm{Mg} = \frac{n_{Mg^{2+}}}{n_{Ca^{2+}} + n_{Mg^{2+}} + n_{SO_4^{2-}}} \times 100 \quad (19)$$

$$\%\,\mathrm{SO_4} = \frac{n_{SO_4^{2-}}}{n_{Ca^{2+}} + n_{Mg^{2+}} + n_{SO_4^{2-}}} \times 100 \quad (20)$$

6.3. Identification of the recovered salts by XRD

All crystallized salts during evaporation are analyzed by XRD technique, Fig. 7 shows the diffractogram of salt crystallized at the end of evaporation (density close to 1.291 g/cm^3) after halite deposit, this salt is essentially composed of epsomite and hexahydrite mixture.

7. Conclusions

Extracting magnesium salts from reverse osmosis discharge was studied in order to reduce its environmental risk.

Different theoretical studies were adopted to predict the crystallization of these salts. Indeed, Phreeqc program was used to simulate the different steps of evaporation. Pitzer model was applied to calculate IAP of all electrolytes and quinary diagrams were studied to draw the crystallization path of solid phases during evaporation.

Experimentally, recovered salts were examined by X-Ray diffraction which displays the presence of epsomite and hexahydrite and confirms the results obtained theoretically.

References

[1] H. Khordagui, Environmental Aspects of Brine Reject from Desalination Industry in the ESCWA Region, ESCWA, Beirut, 1997.
[2] S.F. Dweiri, M.I. Badran, An imminent solution for the future water needs in the Aqaba special economic zone (ASEZ), Desalination 152 (2002) 27–39.

[3] M. Ahmed, A. Arakel, D. Hoey, M.R. Thumarukudy, M.F.A. Goosen, M. Al-Haddabi, A. Al-Belushi, Feasibility of salt production from inland RO desalination plant reject brine: A case study, Desalination 158 (2003) 109–117.
[4] J.M. Arnal, M. Sancho, I. Iborra, J.M. Gozálvez, A. Santafé, J. Lora, Concentration of brines from RO desalination plants by natural evaporation, Desalination 182 (2005) 435–439.
[5] S. Behij, K. Djebali, H. Hammi, A.H. Hamzaoui, A. M'nif, Optimisation of epsomite transformation into periclase using experimental design methodology, J. Chemom. 25 (2011) 59–66.
[6] F. Hajbi, H. Hammi, A. M'nif, Reuse of RO desalination plant reject brine, J. Phase Equilib. Diffus. 31 (2010) 341–347.
[7] F. Hajbi, H. Hammi, R. Solimando, A M'nif, Evaporation of a reverse osmosis discharge studied by Pitzer model and solubility phase diagrams, Fluid Phase Equilib. 307 (2011) 126–134.
[8] K.S. Pitzer, Activity coefficients in electrolyte solution, first ed., R.M Pitkowics, (Ed.), CRS Press, Boca Raton, FL, 1979, pp. 209–265.
[9] K.S. Pitzer, Thermodynamic model for aqueous solutions of liquid-like density, J. Miner. Soc. Am. 17 (1987) 97–142.
[10] K.S. Pitzer, B. Bunsen-Ges, The treatment of ionic solutions over the entire miscible range, J. Phys. Chem. 1981, pp. 85, 952.
[11] K.S. Pitzer, J.M. Simonson, Thermodynamics of multicomponent, miscible, ionic systems: theory and equations, J. Phys. Chem. 90 (1986) 3005.
[12] L.N. Plummer, D.L. Parkhurst, G.W. Fleming, S.A. Dunkle, A Computer Program Incorporating Pitzer's Equations for Calculations of Geochemical Reactions in Brines, U.S.Geological survey. Water-resources Investigations Report, Reston, Virginia, 88 (1988) 4153.
[13] K.S. Pitzer, Ion interaction Approach: Theory and Data Correlation, in: K.S. Pitzer (Ed.), Activity coefficients in Electrolyte Solutions, CRC Press, Boca Raton, 1991, pp. 75–153.
[14] R.T. Pabalan, K.S. Pitzer, Mineral solubilities in electrolyte solutions, in: K.S. Pitzer (Ed.), Activity Coefficients in Electrolyte Solutions, CRS Press, Boca Raton. 1991, pp 435–490.
[15] C.E. Harvie, J.H. Weare, The prediction of mineral solubilities in natural waters: The Na-K-Mg-Ca-Cl-SO_4-H_2O systems from zero to high concentration at 25°C, Geochim. Cosmochim. Acta 44 (1980) 981–997.
[16] G.M. Marion, R.E. Farren, Mineral solubilities in the Na-K-Mg-Ca-Cl-SO4-H2O system: A re-evaluation of the sulfate chemistry in the Spencer-Moller-Weare model, Geochim. Cosmochim. Acta 63 (1999) 1305–1318.
[17] K.S. Pitzer, Thermodynamics of electrolytes. Effects of higher-order electrostatic terms, J. Solution Chem. 4 (1975) 245–265.
[18] A.R. Felmy, J.H. Weare, The prediction of borate mineral equilibria in natural waters: Application to Searles Lake, California, Geochim. Cosmochim. Acta 50 (1986) 2771–2783.
[19] E. Janecke, Ergaänzung zu der neuen Darstellungsform der van't Hoffschen Untersuchungen (Complement to the new form of the van't Hoff's investigations), Z. Anorg. Allgem. Chem. 53 (1907) 319.
[20] J. d'Ans, Die Losungsgleichgewichte der Systeme der Salze Ozeanischer Salzablagerungen 2545 Kali-Forschung sanstalt (The solution equilibria of systems of Oceanic salt deposits 2545 Potash Research sanstalt), Verl. ges. F. Ackerbau, 1933.
[21] A. Droubi, B. Fritz, Y. Tardy, Equilibres entre minéraux et solutions. Programmes de calcul appliqués à la prédiction de la salure des sols et des doses optimales d'irrigation (Equilibria between minerals and solutions. Computer programs applied to the prediction of soil salinity and optimal irrigation doses), Cah.ORSTOM, Ser.Pédol. 14 (1976) 13–38.

Appendix 1. Example of simulation step by PhreeqC interactive.

DATABASE C:\Program Files\USGS\Phreeqc Interactive 2.17.4799\database\pitzer.dat

Initial solution 1. RO discharge

Solution composition

Elements	Molality	Moles
Ca	1.755e – 002	1.053e – 001
Cl	8.212e – 001	4.927e + 000
K	1.737e – 002	1.042e – 001
Mg	9.029e – 002	5.417e – 001
Na	6.548e – 001	3.929e + 000
S (6)	4.709e – 002	2.825e – 001

Phase	Saturation indices			
	SI	log IAP	log KT	
Anhydrite	−0.57	−4.93	−4.36	$CaSO_4$
Arcanite	−4.67	−6.45	−1.78	K_2SO_4
Bischofite	−6.77	−2.31	4.46	$MgCl_2{\cdot}6H_2O$
Bloedite	−5.06	−7.41	−2.35	$Na_2Mg(SO_4)_2{\cdot}4H_2O$
Brucite	−4.77	−15.65	−10.88	$Mg(OH)_2$
Carnallite	−8.91	−4.58	4.33	$KMgCl_3{\cdot}6H_2O$
Epsomite	−2.36	−4.25	−1.88	$MgSO_4{\cdot}7H_2O$
Glaserite	−7.47	−11.28	−3.80	$NaK_3(SO_4)^2$
Glauberite	−2.88	−8.13	−5.25	$Na_2Ca(SO_4)^2$
Gypsum	−0.37	−4.95	−4.58	$CaSO_4{\cdot}2H_2O$
H2O(g)	−1.52	−0.01	1.51	H_2O
Halite	−2.21	−0.64	1.57	NaCl
Hexahydrite	−2.60	−4.23	−1.63	$MgSO_4{\cdot}6H_2O$
Kainite	−6.27	−6.46	−0.19	$KMgClSO_4{\cdot}3H_2O$
Kieserite	−4.05	−4.17	−0.12	$MgSO_4{\cdot}H_2O$
Labile_S	−5.68	−11.35	−5.67	$Na_4Ca(SO_4)^3{\cdot}2H_2O$
Leonhardite	−3.32	−4.21	−0.89	$MgSO_4{\cdot}4H_2O$
Leonite	−6.68	−10.66	−3.98	$K_2Mg(SO_4)^2{\cdot}4H_2O$
Mirabilite	−2.10	−3.32	−1.21	$Na_2SO_4{\cdot}10H_2O$
Misenite	−64.60	−75.40	−10.81	$K_8H_6(SO_4)^7$
Pentahydrite	−2.94	−4.22	−1.28	$MgSO_4{\cdot}5H_2O$
Polyhalite	−6.75	−20.49	−13.74	$K2MgCa_2(SO_4)^4{\cdot}2H_2O$
Portlandite	−11.22	−16.41	−5.19	$Ca(OH)_2$
Schoenite	−6.36	−10.68	−4.33	$K_2Mg(SO_4)^2{\cdot}6H_2O$
Sylvite	−3.17	−2.27	0.90	KCl
Syngenite	−3.94	−11.39	−7.45	$K_2Ca(SO_4)^2{\cdot}H_2O$

(*Continued*)

Appendix 1. (*Continued*)

```
  Reading input data for simulation 2.
  Reaction 1
  H2O(g)    – 30.4
  1 moles in 1 steps
  USE solution 1
  SAVE solution 3
  END
Reaction step 1.

Using solution 1. RO discharge
Using reaction 1.
```

Reactant	Relative moles
$H_2O(g)$	−30.40000

Element	Relative moles
H	−60.80000
O	−30.40000

Solution composition

Elements	Molality	Moles
Ca	1.931e – 002	1.053e – 001
Cl	9.037e – 001	4.927e + 000
K	1.911e – 002	1.042e – 001
Mg	9.936e – 002	5.417e – 001
Na	7.206e – 001	3.929^{e} + 000
S	5.181e – 002	2.825e – 001

Saturation indicies

Phase	SI	log IAP	log KT	
Anhydrite	−0.51	−4.88	−4.36	$CaSO_4$
Arcanite	−4.59	−6.37	−1.78	K_2SO_4
Bischofite	−6.65	−2.20	4.46	$MgCl_2{\cdot}6H2O$
Bloedite	−4.92	−7.27	−2.35	$Na_2Mg(SO_4)^2{\cdot}4H_2O$
Brucite	−4.73	−15.61	−10.88	$Mg(OH)_2$
Carnallite	−8.72	−4.39	4.33	$KMgCl_3{\cdot}6H_2O$
Epsomite	−2.32	−4.20	−1.88	$MgSO4{\cdot}7H2O$
Glaserite	−7.30	−11.11	−3.80	$NaK_3(SO_4)^2$
Glauberite	−2.74	−7.99	−5.25	$Na_2Ca(SO_4)^2$
Gypsum	−0.32	−4.90	−4.58	$CaSO_4{\cdot}2H_2O$
H2O(g)	−1.52	−0.01	1.51	H_2O
Halite	−2.13	−0.56	1.57	NaCl
Hexahydrite	−2.55	−4.19	−1.63	$MgSO_4{\cdot}6H_2O$
Kainite	−6.14	−6.34	−0.19	$KMgClSO_4{\cdot}3H_2O$
Kieserite	−4.00	−4.12	−0.12	$MgSO_4{\cdot}H_2O$
Labile_S	−5.45	−11.12	−5.67	$Na_4Ca(SO_4)^3{\cdot}2H_2O$

(*Continued*)

Appendix 1. (*Continued*)

Reactant	Relative moles			
Leonhardite	−3.27	−4.16	−0.89	$MgSO_4{\cdot}4H_2O$
Leonite	−6.55	−10.53	−3.98	$K_2Mg(SO_4)^2{\cdot}4H_2O$
Mirabilite	−2.03	−3.24	−1.21	$Na_2SO_4{\cdot}10H_2O$
Misenite	−64.23	−75.03	−10.81	$K_8H_6(SO_4)^7$
Pentahydrite	−2.89	−4.17	−1.28	$MgSO_4{\cdot}5H_2O$
Polyhalite	−6.51	−20.26	−13.74	$K_2MgCa_2(SO_4)^4{\cdot}2H_2O$
Portlandite	−11.19	−16.38	−5.19	$Ca(OH)_2$
Schoenite	−6.23	−10.55	−4.33	$K_2Mg(SO_4)^2{\cdot}6H_2O$
Sylvite	−3.09	−2.19	0.90	KCl
Syngenite	−3.81	−11.26	−7.45	$K_2Ca(SO_4)^2{\cdot}H_2O$
End of simulation				